

# Magneto-Electric Coupling in Single Crystal $\text{Cu}_2\text{OSeO}_3$ Studied by a Novel Electron Spin Resonance Technique

A. Maisuradze,<sup>1,2,\*</sup> A. Shengelaya,<sup>3</sup> H. Berger,<sup>4</sup> D. M. Djokić,<sup>4</sup> and H. Keller<sup>1</sup>

<sup>1</sup>*Physik-Institut der Universität Zürich, Winterthurerstrasse 190, CH-8057 Zürich, Switzerland*

<sup>2</sup>*Laboratory for Muon Spin Spectroscopy, Paul Scherrer Institut, CH-5232 Villigen PSI, Switzerland*

<sup>3</sup>*Department of Physics, Tbilisi State University, Chavchavadze av. 3, GE-0128 Tbilisi, Georgia*

<sup>4</sup>*Institute of Condensed Matter Physics, École Polytechnique Fédérale de Lausanne (EPFL), CH-1015 Lausanne, Switzerland*

The magneto-electric (ME) coupling on spin-wave resonances in single-crystal  $\text{Cu}_2\text{OSeO}_3$  was studied by a novel technique using electron spin resonance combined with electric field modulation. An external electric field  $\mathbf{E}$  induces a magnetic field component  $\mu_0 H^i = \gamma E$  along the applied magnetic field  $\mathbf{H}$  with  $\gamma = 0.7(1) \mu\text{T}/(\text{V}/\text{mm})$  at 10 K. The ME coupling strength  $\gamma$  is found to be temperature dependent and highly anisotropic.  $\gamma(T)$  nearly follows that of the spin susceptibility  $J^M(T)$  and rapidly decreases above the Curie temperature  $T_c$ . The ratio  $\gamma/J^M$  monotonically decreases with increasing temperature without an anomaly at  $T_c$ .

PACS numbers: 75.85.+t, 76.50.+g, 76.30.-v

Magneto-electric (ME) materials exhibiting coupled and microscopically coexisting magnetic ( $\mathbf{M}$ ) and electric ( $\mathbf{P}$ ) polarizations have attracted considerable interest in recent years [1–4]. This coupling allows one to influence the magnetic state of a ME material via an external electric field, thus opening a broad range of possible technical applications of such materials [3, 5]. Moreover, it is very interesting to investigate the microscopic mechanism of ME coupling, since  $\mathbf{P}$  and  $\mathbf{M}$  tend to exclude each other [4]. In order to detect the ME effect, sensitive and reliable experimental techniques are required, since this coupling is generally quite small. Usually, for the determination of the ME coupling either the dielectric properties of ME materials are measured as a function of magnetic field or the magnetization is studied as a function of an applied electric field [3].

$\text{Cu}_2\text{OSeO}_3$  is a paraelectric ferrimagnetic material with a Curie temperature of  $T_c \simeq 57$  K [6–8]. The ME effect in  $\text{Cu}_2\text{OSeO}_3$  was first observed by magneto-capacitance experiments [6]. Later on, a small abrupt change of the dielectric constant below  $T_c$  was reported by infrared reflection and transmission studies [9, 10]. Recent  $\mu\text{SR}$  investigations showed a rather small change of the internal magnetic field by applying an electric field [8]. X-ray diffraction [6] and nuclear magnetic resonance [11] studies revealed no evidence of any lattice anomaly below  $T_c$ , suggesting that lattice degrees of freedom are not directly involved in the ME effect. Moreover, a metastable magnetic transition with enhanced magneto-capacitance was observed [6] and later on was also investigated under hydrostatic pressure [12]. Very recently, ME skyrmions were observed in  $\text{Cu}_2\text{OSeO}_3$  by means of Lorentz transmission electron microscopy [13] and small angle neutron scattering [14].

Here we report a study of the ME coupling in single crystal of  $\text{Cu}_2\text{OSeO}_3$ . For this investigation a novel microscopic method for the direct determination of the ME effect based on the standard FMR/EPR technique com-

bined with electric field modulation was developed. As a result, to our knowledge for the first time spin-wave resonance (SWR) excitations [15] were detected via ME coupling. The linear ME coupling strength  $\gamma$  was determined quantitatively in  $\text{Cu}_2\text{OSeO}_3$ . In particular, the temperature and angular dependence of  $\gamma$  and the SWR excitations were investigated. The temperature dependence of the ME coupling was found to follow nearly that of the spin susceptibility without a sudden change across  $T_c$ . By comparing the results of ME  $\text{Cu}_2\text{OSeO}_3$  with those of standard DPPH ( $\text{C}_{18}\text{H}_{12}\text{N}_5\text{O}_6$ ) we further demonstrate that this novel microscopic method is a very sensitive and powerful tool to investigate the ME effect and to search for new ME materials.

High quality single crystals of  $\text{Cu}_2\text{OSeO}_3$  were prepared using a procedure described elsewhere [11]. The crystal structure is cubic with symmetry ( $\text{P}2_13$ ) [6, 7]. Several thin single-crystal samples of approximate dimensions of  $\sim 1 \times 1 \times d$  mm with thickness  $d \leq 0.1$  mm were studied. The [110] direction of the crystal is oriented perpendicular to the planes of the thin samples (see Fig. 1a). The FMR and EPR measurements were performed with a standard X-band (9.6 GHz) *BRUKER EMX* spectrometer. In order to detect the ME effect a capacitor-like structure consisting of two thin ( $< 10 \mu\text{m}$ ) isolated gold electrodes separated by  $\simeq 0.3$  mm was used (see Fig. 1a). The sample and the DPPH marker [16, 17] were placed between the two electrodes. The electrodes were connected to an ac voltage source of amplitude  $V_m = 17$  V, synchronized with the frequency of 100 kHz of the magnetic field modulation generator of the spectrometer [16, 17]. Two kind of resonance experiments were performed: (1) EPR/FMR with standard magnetic field modulation (MFM) and (2) EPR/FMR with electric field modulation (EFM) at 100 kHz. The [110] axis of the crystal was perpendicular to the microwave field  $\mathbf{H}_1$ . For the angular dependent measurements the sample was rotated with respect to the applied field  $\mathbf{H}$  (see Fig. 1a).

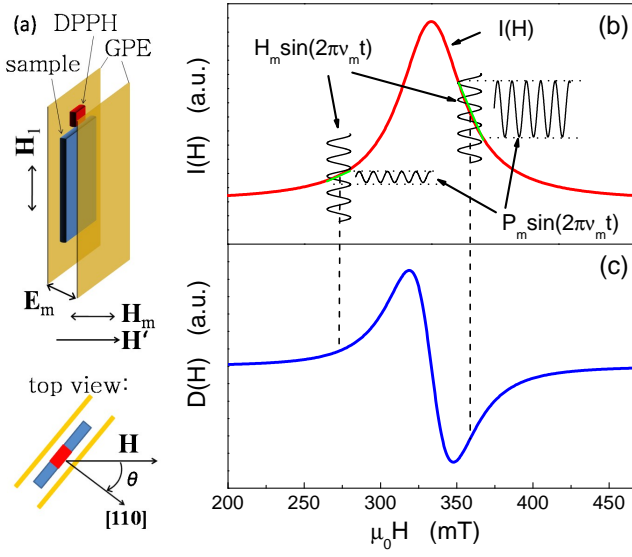


FIG. 1: (Color online) (a) Schematic view of the sample and the magnetic/electric field geometry. The ME sample and the marker sample DPPH are sandwiched between two gold plate electrodes (GPE).  $H'$ : static external magnetic field,  $H_m$ : magnetic modulation field,  $E_m$ : electric modulation field,  $H_1$ : microwave field,  $H = H' + H_m$ : total external magnetic field. (b) Basic principle of EPR signal detection. Red curve represents the EPR absorption line  $I(H)$ . The modulation magnetic field  $H_m \sin(2\pi\nu_m t)$  and the resulting modulated microwave absorption power  $P_m \sin(2\pi\nu_m t)$  are also illustrated. (c) First derivative  $D(H)$  signal of the EPR absorption line  $I(H)$  after lock-in detection.

The EPR/FMR technique is based on the resonance absorption of microwave energy by a Zeeman-split spin system [16, 17]. The Zeeman splitting of the spin system is achieved by sweeping an applied magnetic field  $H$ . In the simplest case of an effective spin  $S = 1/2$  system (as for the present case of  $\text{Cu}^{2+}$ ) the double degenerate ground state is split into two levels by the Zeeman energy  $E_Z = g\mu_B H$ . When  $E_Z = h\nu$ , where  $\nu = 9.6$  GHz is the frequency of the microwave  $H_1$  field, resonance absorption takes place (see Fig. 1b). In order to increase the sensitivity, the applied magnetic field  $H$  is modulated:  $H = H' + H_m \sin(2\pi\nu_m t)$ , where  $H'$  is the static applied magnetic field,  $H_m$  is the modulation amplitude, and  $\nu_m$  is the modulation frequency (typically  $\nu_m = 100$  kHz). During signal detection  $H'$  is swept slowly. As a result, the detected microwave absorption power  $P(t) = P_m \sin(2\pi\nu_m t)$  is also modulated with the frequency  $\nu_m$ . The amplitude  $P_m$  is proportional to the slope  $D(H)$  of the absorption signal  $I(H)$ . Further amplification and lock-in detection of  $P(t)$  results in the EPR derivative signal  $D(H)$  as illustrated in Fig. 1c [16, 17].

Ferromagnetic resonance studies were performed previously on composite ME structures involving piezoelectric and magnetostrictive compounds [18–20]. In these experiments a static external field  $E_{st}$  was used to de-

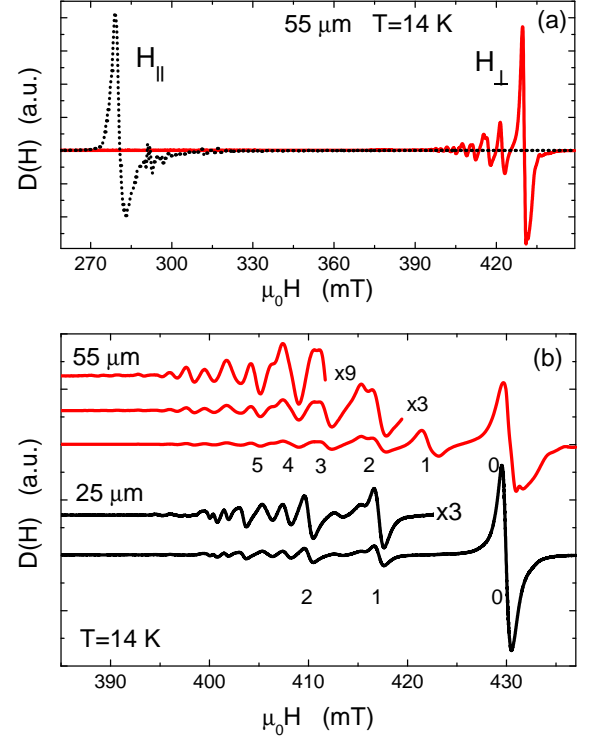


FIG. 2: (Color online) (a) FMR in the 55  $\mu\text{m}$  thick single-crystal sample of  $\text{Cu}_2\text{OSeO}_3$  at  $T = 14$  K for  $H_{||}$  and  $H_{\perp}$  using the conventional MFM technique. (b) SWR in the 25 and 55  $\mu\text{m}$  thick single-crystal samples of  $\text{Cu}_2\text{OSeO}_3$  at  $T = 14$  K for  $H_{\perp}$ . The indices 0, 1, 2, ... indicate the order of the SWR mode.

tect the ME coupling strength. By applying  $E_{st} = 1$  kV/mm in the present experiments a shift of the resonance fields of the order of  $\simeq 0.5$  mT was also detected for  $\text{Cu}_2\text{OSeO}_3$ , indicating an additional magnetization induced by  $E_{st}$  (see supplemental materials). However, in order to increase the sensitivity of signal detection and to avoid artifacts related to hysteresis effects of the magnet core it is advantageous to apply a periodic voltage to detect small changes in the spectra. This technique was previously applied to investigate the electric field effect on the non-Kramers ion  $\text{Pr}^{3+}$  in  $\text{LaMgN}_2$  [21]. The main idea of the present experiment is to use EFM to observe EPR/FMR signals in  $\text{Cu}_2\text{OSeO}_3$  instead of the usual MFM technique. In a spin system without ME effect (e.g. DPPH) no modulated signal  $P(t) = P_m \sin(2\pi\nu_m t)$  will occur. However, if the ME effect is present in the sample, modulation by an electric field  $E_m \sin(2\pi\nu_m t)$  leads to a modulation of the magnetization  $M(t)$  and therefore to a modulation of the magnetic field in the sample  $B(t) = \mu_0[H + M(t)]$ . In this case the EPR/FMR signal which is proportional to the ME coupling may in principle be detected.

First we describe the FMR/EPR signals obtained in  $\text{Cu}_2\text{OSeO}_3$  using the conventional MFM technique. For

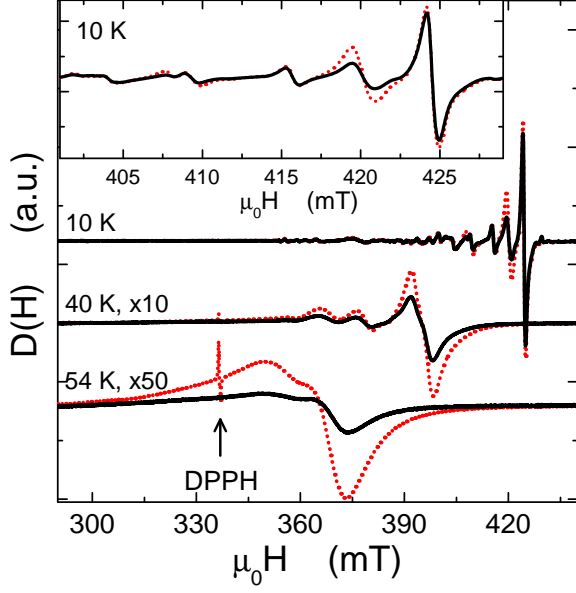


FIG. 3: (Color online) Temperature dependence of SWR signals of single-crystal  $\text{Cu}_2\text{OSeO}_3$  detected using the MFM technique (dotted line) and the EFM technique (solid line). The sharp peak visible at 340 mT and 54 K is the signal of the marker sample DPPH which is present only in the case of MFM. The inset shows the expanded spectra at 10 K around 415 mT. For better comparison all the EFM signals are multiplied by a factor of 2.

a polycrystalline or arbitrarily shaped single crystal a very complex signal is observed as reported previously (see Ref. [22]). We found that the signal is substantially simpler for a thin single crystal with a nearly constant effective demagnetization factor [23]. Figure 2a shows the FMR signal of a thin single-crystal sample of  $\text{Cu}_2\text{OSeO}_3$  (thickness  $d = 55 \mu\text{m}$ ) at 14 K with the applied magnetic field  $H$  parallel ( $H_{\parallel}, \theta = 90^\circ$ ) and perpendicular ( $H_{\perp}, \theta = 0^\circ$ ) to the plane of the sample (see Fig. 1a). For  $H_{\parallel}$  a slightly skewed single signal is observed, whereas for  $H_{\perp}$  multiple peaks with different signal intensities are evident. These peaks represent resonances of different spin-wave (SW) modes. In thin ferromagnetic samples SW modes are expected to occur at resonance fields  $H_n$  [15, 24, 25]:

$$H_n = H_0 - S \left( \frac{\pi}{d} \right)^2 [(n+1)^2 - 1] \quad (1)$$

Here,  $S$  is a parameter related to the spin stiffness [15, 24],  $n$  is the order of the spin-wave mode, and  $d$  is the thickness of the sample. With increasing  $n$  the resonance field  $H_n$  decreases, and with decreasing  $d$  the difference  $H_0 - H_1$  increases. Qualitatively this behavior agrees with our observation (see Fig. 2b). However, there are quantitative deviations from Eq. (1) as was reported previously for various materials [24, 25]. These deviations are often related to stress, magnetic anisotropy, distribution or variation of magnetization across the sample.

As shown in Fig. 2 it was possible to detect SW modes with order  $n > 10$  in the present experiments. However, due to a slight variation of thickness  $d$  across the sample the modes of high order  $n$  interfere. Moreover, with increasing temperature the linewidths of the SWR modes increase and overlap (see Fig. 3).

Next we discuss the ME effect using the EFM method by applying an ac electric field  $E_m \sin(2\pi\nu_m t)$ . Figure 3 shows some typical FMR spectra of the  $55 \mu\text{m}$  thick single-crystal sample at different temperatures detected by this technique. It is evident that the SWR lines are also observed as for MFM. At 10 K the SWR signals  $D^M(H)$  and  $D^E(H)$  detected by MFM and EFM, respectively, have approximately the same amplitudes. With increasing temperature, however, the amplitude of  $D^E(H)$  is reduced compared to that of  $D^M(H)$ . Above 60 K the intensity of the  $D^E(H)$  signal becomes very small. Note that for the marker sample DPPH no signal is present in the case of EFM as expected. The absence of a DPPH signal unambiguously demonstrates that ME coupling in  $\text{Cu}_2\text{OSeO}_3$  gives rise to the  $D^E(H)$  signal (see also supplemental materials). Thus, the ratio of the signal intensities detected by electric and magnetic modulations is proportional to strength of the ME effect [26]:

$$\alpha(H) = \frac{I^E(H)}{I^M(H)} \equiv \frac{\int_0^H D^E(h)dh}{\int_0^H D^M(h)dh}. \quad (2)$$

This ratio is determined by  $\alpha = \mu_0 H^i / \mu_0 H_m$ , where  $\mu_0 H_m^i = \gamma E_m$  is the magnetic field induced by the electric field  $E_m$  and  $\mu_0 H_m = 0.1 \text{ mT}$  is the field used in the MFM experiment. Therefore, the ME coupling strength  $\gamma = \alpha C$  with a calibration factor  $C = \mu_0 H_m / E_m = 1.76 \mu\text{T}/(\text{V}/\text{mm})$  [1, 3]. It is convenient to introduce the spectrally averaged value of  $\alpha(H)$ :

$$\langle \alpha \rangle = \frac{\int I^M(H) \alpha(H) dH}{\int I^M(H) dH} = \frac{\int I^E(H) dH}{\int I^M(H) dH} = \frac{J^E}{J^M}. \quad (3)$$

Here,  $J^\beta = \iint D^\beta(h) d^2h$ , ( $\beta = E, M$ ) are the signal intensities in the EFM and the MFM experiments, respectively.  $J^M$  is also a measure of spin susceptibility [16]. The temperature dependence of  $\alpha(H)$  for  $H_{\perp}$  is shown in Fig. 4a. Above 20 K  $\alpha(H)$  has a minimum at around 300 mT, and is nearly constant above 320 mT. The averaged ME effect parameter  $\langle \alpha \rangle$  as a function of temperature is plotted in Fig. 4b, together with the temperature dependencies of  $J^E$  and  $J^M$ . The ME effect is most pronounced at low temperatures and decreases with increasing temperature. With the above value of  $C$  and  $\langle \alpha \rangle = 0.4$  one obtains  $\gamma = 0.7(1) \mu\text{T}/(\text{V}/\text{mm})$  at 10 K. Below 20 K the ME effect is decreasing slightly faster than  $J^M$  with increasing temperature as shown in Fig. 4b. Above 60 K the ME effect rapidly decreases, although it is still present in the paramagnetic phase. The insert of Fig. 4b shows  $\langle \alpha \rangle$  at 14 K as a function

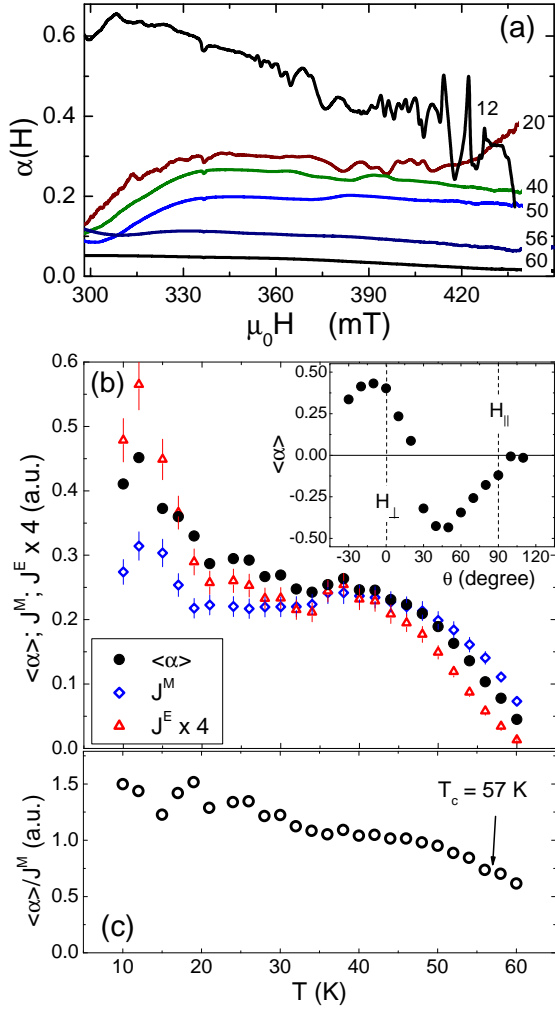


FIG. 4: (Color online) (a) Spectrally resolved ME effect parameter  $\alpha(H)$  in single-crystal  $\text{Cu}_2\text{OSeO}_3$  at  $T = 12, 20, 40, 50, 56$ , and  $60$  K for  $H_{\perp}$ . (b) Temperature dependence of the average ME effect parameter  $\langle\alpha\rangle$  and the signal intensities  $J^E$  and  $J^M$  detected by EFM and MFM, respectively. The inset shows the angular dependence of  $\langle\alpha\rangle$  at  $14$  K. (c) Temperature dependence of the ratio  $\langle\alpha\rangle/J^M$  showing no anomaly at  $T_c$ .

of the angle  $\theta$  (see Fig. 1a). The sign change of  $\langle\alpha(\theta)\rangle$  at  $\theta \simeq 25^\circ$  corresponds to the change of the direction of the induced magnetization  $M^i$  with respect to  $\mathbf{H}$ . The observed  $\langle\alpha(\theta)\rangle$  indicates that the ME effect depends not only on the relative orientation of  $\mathbf{E}_m$  and  $\mathbf{H}$  (see Fig. 1a), but also on the crystal orientation with respect to these fields. In Fig. 4c the temperature dependence of the ratio  $\langle\alpha\rangle/J^M$  is shown. This ratio decreases gradually with increasing temperature showing no anomaly at  $T_c = 57$  K indicating that ME coupling mechanism is not related to the onset of long range magnetic order. The ME coupling is linear as is evident from the linear relation between the SWR peak-to-peak amplitude  $A_{pp}$  of  $D(H)$  and the applied EFM amplitude  $E_m$  (see Figs.

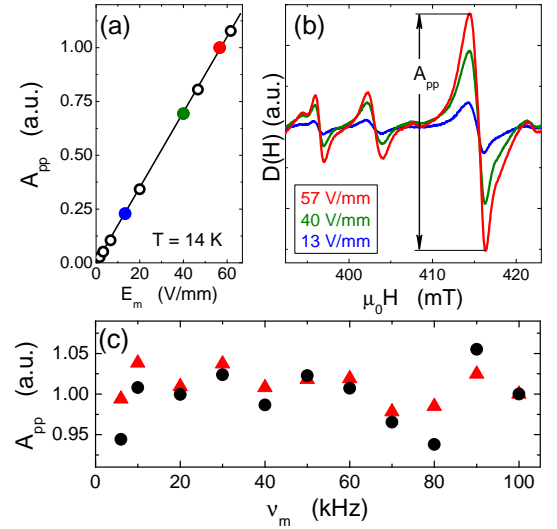


FIG. 5: (Color online) (a) Peak-to-peak amplitude  $A_{pp}$  of the zero order SWR mode extracted from  $D(H)$  shown in (b) as a function of the EFM amplitude  $E_m$  in  $\text{Cu}_2\text{OSeO}_3$ . Note that  $A_{pp} \propto E_m$  indicating that ME coupling is linear. (c)  $A_{pp}$  as a function of the EFM frequency  $\nu_m$  at  $T = 25$  K ( $\bullet$ ) and  $35$  K ( $\blacktriangle$ ).

5a and 5b). In Fig. 5c we show  $A_{pp}$  as a function of the EFM frequency  $\nu_m$ . Note that  $A_{pp}$  shows no appreciable frequency dependence, indicating that  $\gamma$  is not related to a mechanical resonance of the sample, as observed in some of the composite ME materials [27].

It is interesting to compare the magnitude of the ME effect  $\gamma = \alpha C$  observed in this work with previous results [6, 8]. For an applied electric field of  $\delta E = 500/3$  (V/mm) a change of the internal magnetic field of  $\mu_0 \delta H_{\mu\text{SR}}^i = 0.4(4)$  mT was detected by  $\mu\text{SR}$  [8]. This corresponds to an electric field induced magnetization of  $\mu_0 \delta \overline{M}_{\mu\text{SR}} = \mu_0 \delta H_{\mu\text{SR}}^i (1 - N)^{-1} \simeq 0.6$  mT (for  $N = 1/3$  [28]). For the same electric field and for a mean value of  $\langle\alpha\rangle \simeq 0.28$  for  $T < 50$  K, the average induced magnetization is estimated to be  $\mu_0 \delta \overline{M}_{\text{FMR}} = \mu_0 \delta H_{\text{FMR}}^i (1 - N)^{-1} = \langle\alpha\rangle C \delta E (1 - N)^{-1} \simeq 0.55$  mT, where  $N \simeq 0.85$  was used corresponding to the actual geometry of the sample [23]. The present value of  $\mu_0 \delta \overline{M}_{\text{FMR}} \simeq 0.55$  mT is in good agreement with the value of  $\simeq 0.6$  mT obtained by  $\mu\text{SR}$  [8]. The observed temperature dependence of the ME effect differs slightly from that measured by magneto-capacitance experiments on powder samples [6], but it is in agreement with that observed recently for a single crystal sample [29]. While the ME effect parameter  $\langle\alpha\rangle$  is strongly reduced above  $60$  K, the ME effect reported in Ref. [6] is still substantial up to  $65$  K.

In summary, the magneto-electric coupling in single crystal of  $\text{Cu}_2\text{OSeO}_3$  was studied by means of a novel and highly sensitive magnetic resonance technique. This method is based on the use of electric field modulation in-

stead of conventional magnetic field modulation in standard continuous wave EPR. Resonance lines of spin wave modes of more than order 10 could be resolved in the FMR spectra. Moreover, spin wave resonances were observed via the ME coupling by applying an electric field modulation technique. By combining magnetic and electric field modulation experiments, the temperature and angular dependence of the linear ME effect in  $\text{Cu}_2\text{OSeO}_3$  was investigated for the electric field parallel to the [110] direction of the crystal. The ME coupling was found to be  $\gamma = 0.7(1) \mu\text{T}/(\text{V}/\text{mm})$  at 10 K. The magnetization induced by the applied electric field is in good agreement with previous  $\mu\text{SR}$  results [8]. The temperature dependence of the ratio of ME coupling strength to the spin susceptibility  $\gamma/J^M$  exhibits no anomaly at  $T_c = 57$  K. This indicates that the ME coupling mechanism is not related to the presence of long range magnetic order.

We acknowledge support by the Swiss National Science Foundation, the NCCR Project *Materials with Novel Electronic Properties* (MaNEP), the SCOPES Grant No. IZ73Z0-128242, and the Georgian National Science Foundation Grant GNSF/ST08/4-416.

---

\* Electronic address: alexander.m@physik.uzh.ch

- [1] M. Fiebig, J. Phys. D: Appl. Phys. **38** R123 (2005).
- [2] N. A. Spaldin and M. Fiebig, Science **309**, 391 (2005).
- [3] W. Eerenstein, N.D. Mathur, and J.F. Scott, Nature **442**, 759 (2006).
- [4] N. A. Hill, J. Phys. Chem. B **104**, 6694 (2000).
- [5] M. Bibes and A. Barthélemy, Nature Materials **7**, 425 (2008).
- [6] J.-W. G. Bos, C. V. Colin, and T. T. M. Palstra, Phys. Rev. B **78**, 094416 (2008).
- [7] H. Effenberger and F. Pertlik, Monatsch. Chem. **117**, 887 (1986).
- [8] A. Maisuradze et al., Phys. Rev. B **84**, 064433 (2011).
- [9] K. H. Miller et al., Phys. Rev. B **82**, 144107 (2010).
- [10] V. Gnezdilov et al., Fiz.Nizk. Temp. **36**, 688 (2010).
- [11] M. Belesi et al., Phys. Rev. B **82**, 094422 (2010).
- [12] C.L. Huang et al., Phys. Rev. B **83**, 052402 (2011).
- [13] S. Seki, X. Z. Yu, S. Ishiwata, and Y. Tokura, Science **336**, 198 (2012).
- [14] T. Adams et al., arXiv:1204.3597v1 (2012).
- [15] C. Kittel, Phys. Rev. **110**, 1295 (1958).
- [16] A. Abragam and B. Bleaney, *Electron Paramagnetic Resonance of Transition Ions* (Clarendon, Oxford, 1970).
- [17] Ch. P. Poole, *Electron Spin Resonance: A Comprehensive Treatise on Experimental Techniques* (Dover Publications, 2 ed. 1997).
- [18] Y. Chen et al., Phys. Rev. B **83**, 104406 (2011).
- [19] M. Weiler et al., Phys. Rev. Lett. **106**, 117601 (2011).
- [20] S. Shastry, et al., Phys. Rev. B **70**, 064416 (2004).
- [21] P. Wyssling and K.A. Müller, J. Phys. C: Solid State Phys. **9**, 635 (1976).
- [22] M.I. Kobets et al., Low. Temp. Phys. **36**, 176 (2010).
- [23] G. Zheng et al., J. Appl. Phys. **79**, 5742 (1996).
- [24] T.G. Rappoport, et al., Phys. Rev. B **69**, 125213 (2004).
- [25] X. Liu and J.K. Furdyna, J. Phys.: Condens. Matter **18**, R245 (2006).
- [26] Provided that the rest of experimental conditions are identical.
- [27] U. Laetsin et al., Appl. Phys. A **78**, 33 (2004).
- [28] Assuming an effective demagnetization factor  $N = 1/3$  for a randomly shaped domain.
- [29] M. Belesi et al., arXiv:1204.3783v1 (2012).